Magnetically driven superhydrophobic/superoleophilic graphene-based polyurethane sponge for highly efficient oil/water separation and demulsification

A. Jamsaz, E.K. Goharshadi, Alexandre Barras, M. Ifires, Sabine Szunerits, Rabah Boukherroub

Magnetically driven superhydrophobic/superoleophilic graphene-based polyurethane sponge for highly efficient oil/water separation and demulsification

Azam Jamsaz[a,b], Elaheh K. Goharshadi[a,c,*], Alexandre Barras[b], Madjid Ifires[b,d], Sabine Szunerits,[b] Rabah Boukherroub[b,*]

[a] *Chemistry Department, Faculty of Science, Ferdowsi University of Mashhad, Mashhad 9177948974, Iran*

[b] *Univ. Lille, CNRS, Centrale Lille, Univ. Polytechnique Hauts-de-France, UMR 8520 - IEMN, F-59000 Lille, France*

[c] *Nano Research Center, Ferdowsi University of Mashhad, Mashhad 9177948974, Iran*

[d] *Research Center of Semi-conductor Technology for Energy, CRTSE - 02, Bd. Dr. Frantz FANON, B.P. 140 Algiers-7, Merveilles, 16038, Algeria*

*Corresponding authors.

[*]E-mail: gohari@um.ac.ir (E. K. Goharshadi), rabah.boukherroub@univ-lille.fr (R. Boukherroub)

Abstract

Cost-effective and efficient sorbents with emulsion-breaking capability, especially surfactant-stabilized emulsions, are required to remediate oil spills from water. Herein, *in situ* growth of magnetic $Mn_{0.01}Co_{0.90}Fe_3O_4$ (MCFO) nanoparticles (NPs) on reduced graphene oxide (RGO) was performed to prepare MCFO/RGO nanocomposite *via* a simple solvothermal method. The nanocomposite was coated onto a polyurethane (PU) sponge to fabricate a novel magnetic, superhydrophobic/superoleophilic and flame-retardant material. The prepared magnetic MCFO/RGO/PU was superhydrophobic with a contact angle of 165 ± 1°. Compared with neat PU, the MCFO/RGO/PU sponge could be effectively driven by a magnet for oil collection in water. More importantly, the MCFO/RGO/PU sponge could effectively collect oil droplets from surfactant-free and stabilized toluene/water emulsions. In addition, the fabricated sponge exhibited excellent performance for oils and organic solvents sorption, achieving up to 131 times of its own weight and retaining its ability even after 10 sorption cycles. Interestingly, the thermal stability and fire retardancy of the prepared PU sponge were improved with respect to neat PU.

Keywords: $Mn_{0.01}Co_{0.90}Fe_3O_4$/reduced graphene oxide; magnetic polyurethane sponge; superhydrophobic/superoleophilic; demulsification capacity; flame retardant

1. Introduction

Nowadays, the production of oily wastewater discharged from domestic and industrial activities is extremely increasing. Therefore, the separation of oil/water mixtures and treating oily wastewater resources have become an urgent world challenge. Generally, oil/water mixtures are classified into two categories including immiscible oil-water and miscible oil-water mixtures (oil-in-water (O/W) and water-in-oil (W/O) emulsions). Due to the small size ($d < 20\ \mu m$) and high stability of emulsion droplets, their separation is more challenging and difficult than immiscible oil/water mixtures with average droplet size up to $150\ \mu m$ [1]. As a result, much efforts have been devoted to design novel, low cost, reusable, and recyclable sorbents for oil/water separation.

The most common methods used for the separation of oil/water mixtures are sorption and filtration [2]. Nanocomposites, gels, powders, particles, and porous media are usually used as sorbent materials, while the common filtration materials applied in oil-water separation are films, filters, membranes, and meshes. Although filtration has been used as a successful method in industry, contaminants could not be effectively collected from mixtures. Sorbents, especially 3-dimensional (3D) porous materials, can easily adsorb contaminants from wastewater resources [3]. They are not expensive and there is no need of any specialized equipment to clean up the contaminants. Both natural including cotton fibers, kapok fibers, wool and synthetic sponges (e.g. polyurethane (PU) and melamine sponges), polystyrene fibers, and carbon nanotubes (CNTs) have been widely used as sorbents [2]. Although, natural materials offer some excellent advantages such as high abundance and low cost, they suffer from some shortcomings like flammability, non-reusability, introduction of new pollutants into the contaminated system, and poor sorption capacity. In addition, they are not suitable for separation of emulsified oil/water mixtures, especially in surfactant-stabilized emulsions [4]. In contrast, 3D porous sorbents like PU sponge with its specific features

represents an appealing alternative. PU sponge could act as a promising candidate for oil-water separation, because of its outstanding properties like large surface area, 3D skeleton, porous structure, remarkable flexibility, good sorption capacity, promising reusability, and inter-connected matrix [5-9]. Additionally, for effective oil/water separation, superhydrophobicity (surface with a water contact angle (WCA) higher than 150º) is crucial. Since PU is slightly hydrophobic, its non-wettability should be enhanced [10]. In addition, PU sponge is easily ignited and generates toxic gases [11]. These drawbacks hamper significantly the practical applications of PU sponge in oil-water separation [12]. Therefore, it is necessary to alter surface wettability of PU and make it suitable for oil/water separation processes such as emulsions (W/O and O/W) and highly viscous oil/water mixtures. There are several reports for the preparation of superhydrophobic/superoleophilic PU sponges. For example, Wang et al. [13] prepared a superhydrophobic and flame retardant PU sponge in an aqueous suspension containing alkaline water/ethanol, dopamine, fly ash, and dodecanethiol through the dip-coating method. The modified sponge presented a good oil sorption capacity (34-47 g/g) and separation efficiency for oil-in-water emulsions (93.0%).

To modify PU, graphene-based materials such as reduced graphene oxide (RGO) and graphene oxide (GO) have been utilized, owing to their remarkable physicochemical properties such as low density, large specific surface area, and biocompatibility [14, 15]. Moreover, GO sheets are decorated with hydrophilic functional groups including hydroxyl, epoxy, carbonyl, and carboxylic on their basal planes and edges. The oxygen-containing functional groups of GO can play a main role in modification of PU sponge. Liu et al. [16] synthesized silica NPs on GO surface (SiO_2/GO). Then, PU sponge was dipped into the ethanol/water solution containing the SiO_2/GO to obtain a hydrophobic SiO_2/GO/PU (WCA=145°). The modified PU sponge presented a high sorption capacity of 180 g/g for chloroform and exhibited a high stability for 10 cycles without any change of the intrinsic

structure of the PU sponge. Some of us [15] prepared a flame retardant, superhydrophobic/superoleophilic graphene-based PU sponge by utilizing a simple *in-situ* chemical method. The modified sponge displayed a high sorption capacity of 80 g/g for chloroform and exhibited greater thermal stability with respect to neat PU.

By incorporation of magnetic nanoparticles (NPs) into graphene-based PU sponge, both oil/water separation and fire retardancy properties could be enhanced [17-19]. Moreover, the whole separation process could be controlled through external stimulation using a magnet. Yang et al. [20] fabricated graphene aerogels modified by magnetic carbon nanospheres through one-step hydrothermal *in-situ* electrostatic self-assembling method. The prepared aerogels showed excellent thermal stability, flame retardancy, and magnetic properties. In addition, they achieved high sorption capacity (187–537 g/g) for several organic solvents and oils. Boukherroub et al. [21] prepared a superhydrophobic/superoleophilic PU sponge through a two-step functionalization process. The modified sponge not only presented high sorption capacity (40-75 g/g) for several oils, but it was also successfully applied for effective separation of O/W emulsions.

Herein, we prepared $Mn_{0.01}Co_{0.90}Fe_3O_4$ nanoparticles (MCFO NPs) *via* a simple solvothermal method. Then, the prepared NPs were grown on GO to form MCFO/RGO nanocomposite and incorporated into a PU sponge. Introduction of some magnetic metal ions such as manganese and cobalt ions can affect the thermal degradation and flame-retardancy of PU [22]. To the best our knowledge, this is the first demonstration of the preparation of PU functionalized with MCFO/RGO nanocomposite. The MCFO/RGO/PU sponge displayed excellent superhydrophobic property with high selectivity and outstanding recyclability for oil sorption. It could be magnetically directed to adsorb oils and organic solvents up to 131 times of its weight with respect to neat PU sponge. Additionally, one of the great success of this work is to separate oil droplets from oil-in-water emulsions by the prepared

MCFO/RGO/PU sponge. In fact, oil/water emulsions especially in the presence of surfactants are more difficult to separate in real spaces, as compared to immiscible oil/water mixtures.

2. Experimental

2.1. Preparation of $Mn_{0.01}Co_{0.90}Fe_3O_4$ (MCFO)/RGO nanocomposite

In situ growth of MCFO NPs on GO to produce MCFO/RGO nanocomposite was performed by a facile solvothermal method. For this purpose, 80 mg of GO were dispersed in 80 mL of ethylene glycol and 3 mL of ethyl acetate in an ultrasonic bath for 60 min. Afterwards, $Mn(CH_3COO)_2{\cdot}4H_2O$ (0.5 mmol), $Co(CH_3COO)_2{\cdot}4H_2O$ (0.5 mmol), $FeCl_3{\cdot}6H_2O$ (2.0 mmol), and CH_3COONa (1.2 mmol) were added into the aforementioned mixture and sonicated to form a homogeneous slurry. The mixture was sealed in a stainless-steel autoclave and heated at 200 °C for 72 h. The obtained precipitate was collected by centrifugation and washed with Milli-Q water and ethanol, and finally dried in an oven at 50 °C for 24 h to obtain the MCFO/RGO nanocomposite. The similar procedure was used to prepare magnetic MCFO/RGO nanocomposites with different amounts of GO (70, 80, and 90 mg). The resulting nanocomposites are denoted as MCFO/RGO-1 (GO=70 mg), MCFO/RGO-2 (GO=80 mg), and MCFO/RGO-3 (GO=90 mg).

2.2. Preparation of magnetic MCFO/RGO/PU sponge

PU sponge pieces (1×1×1 cm^3) were washed first with acetone and then with DI water in an ultrasonic bath for 10 min and dried in an oven for 2 h at 80 °C. The clean sponge was dipped in a solution containing MCFO/RGO-1 (50 mg), ethanol (10 mL), and Milli-Q (10 mL) and maintained under stirring for 6 h at room temperature. After that, the treated sponge was dried by freeze-drying for 5 h. A similar approach was applied for the preparation of MCFO/RGO-2 and 3 samples. Similarly, three sponges denoted as MCFO/RGO/PU-1

(GO=70 mg), MCFO/RGO/PU-2 (GO=80 mg) and MCFO/RGO/PU-3 (GO=90 mg) were prepared.

2.3. Preparation of RGO/PU sponge

GO (80 mg) was dispersed in water (80 mL) and sealed in a stainless-steel autoclave and heated at 200 °C for 72 h to prepare RGO powder. A clean PU sponge was dipped into the solution containing RGO (50 mg), ethanol (10 mL), and Milli-Q (10 mL) and maintained under stirring for 6 h at room temperature. Finally, the treated sponge was dried by freeze-drying for 5 h.

2.4. Oil and solvent sorption

The sorption capacity, Q, (mass/mass, g/g) of neat PU, RGO/PU, and MCFO/RGO/PU sponges for oils and organic solvents including cooked oil, chloroform, toluene, ethyl acetate, and dichloromethane was measured at room temperature. The sorption capacity was calculated using Eq. 1:

$$Q = \frac{m_1 - m_0}{m_0} \quad (1)$$

where m_0 and m_1 represent respectively the mass of MCFO/RGO/PU sponge before and after sorption.

2.5. Emulsion separation using MCFO/RGO/PU sponge

2.5.1. Surfactant-free water-in-oil emulsion (W/O)

Water (1 mL) was added to toluene (9 mL) and sonicated for 1 h to produce a milky white solution. The MCFO/RGO/PU sponge (1×1×1 cm^3) was immersed in 4 mL of the emulsion for 30 min till the emulsion became colorless. The content of toluene in water was determined using a calibration curve generated from the UV–vis absorbance spectra at 260

nm of different concentrations of toluene dispersed in methanol/water (3/1, v/v) solution (**see SI**).

2.5.2. Surfactant-stabilized oil-in-water emulsion (O/W)

Pluronic F-127 (0.1 mg/mL in water) was added to toluene/water (1:9, v/v) and sonicated for 1 h to prepare a milky white solution. The MCFO/RGO/PU sponge (1×1×1 cm^3) was immersed in 4 mL of the emulsion for 30 min till the emulsion became colorless. The content of toluene in water was determined as above.

3. Results and discussion

3.1. Preparation of magnetic superhydrophobic/superoleophilic (MCFO/RGO/PU) sponge

MCFO/RGO/PU sponge was fabricated through a two-step process including a solvothermal method to coat MCFO NPs on RGO nanosheets, followed by dip-coating method to load MCFO/RGO nanocomposite onto the PU surface. The preparation process of MCFO/RGO nanocomposite is illustrated in **Figure S1**. The well-dispersed GO nanosheets in ethylene glycol and ethyl acetate solution served as a substrate for the nucleation and *in situ* growth of MCFO NPs [23]. Co^{2+}, Mn^{2+}, and Fe^{3+} ions can be anchored on the GO surface during the nucleation process through electrostatic interactions between the positively charged metal ions and the negatively charged GO sheets [24, 25]. By elapsing time, GO was partially reduced to RGO and NPs were formed around the heterogeneous nucleation sites on the RGO sheets [26]. The solvents may act as structure-directing agents and prevent agglomeration of the NPs during the nucleation step. Finally, MCFO/RGO/PU nanocomposite was prepared by immersion of a PU sponge into a MCFO/RGO colloidal solution. ~~The sponge and nanocomposite were connected through hydrogen bonding between –HNCO– groups of PU and the deprotonated oxygen-functional groups of MCFO/RGO. In addition, $\pi - \pi$ stacking interactions between RGO sheets and aromatic groups of PU sponge~~

~~could strengthen the bonding of MCFO/RGO nanocomposite on the PU surface.~~ The MCFO nanoparticles are strongly immobilized on the RGO surface owing to the presence of plenty of oxygen-containing groups on the GO precursor. The MCFO/RGO is in turn adsorbed on PU surface through π–π stacking interactions between RGO sheets and aromatic groups of the PU sponge.

3.2. Characterization

3.2.1. WCA measurements

To investigate the wetting properties of neat PU and prepared sponges including RGO/PU, MCFO/RGO/PU-1, MCFO/RGO/PU-2, and MCFO/RGO/PU-3, the WCA was measured on three different locations on the surface of the sponges using 4 μL of DI water droplets at room temperature. As shown in **Figure 1**, neat PU sponge displays a WCA of 108 ± 1°, which increased to 129 ± 1° after RGO coating. The hydrophobicity of the PU sponge was enhanced upon loading MCFO/RGO on its surface, as witnessed by the apparent WCA values of MCFO/RGO/PU-1 (151 ± 1°), MCFO/RGO/PU-2 (165 ± 1°) and MCFO/RGO/PU-3 (143 ± 1°). It is obvious that the WCA of MCFO/RGO/PU-2 herein after named as MCFO/RGO/PU is greater than those of other modified sponges. By increasing the amount of GO above 80 mg, the WCA decreased. It is believed that higher amounts of GO can fill the pores of the PU sponge and decrease its surface roughness and wettability. Also, it is likely that RGO nanosheets are aggregated with increasing the amount of GO precursor.

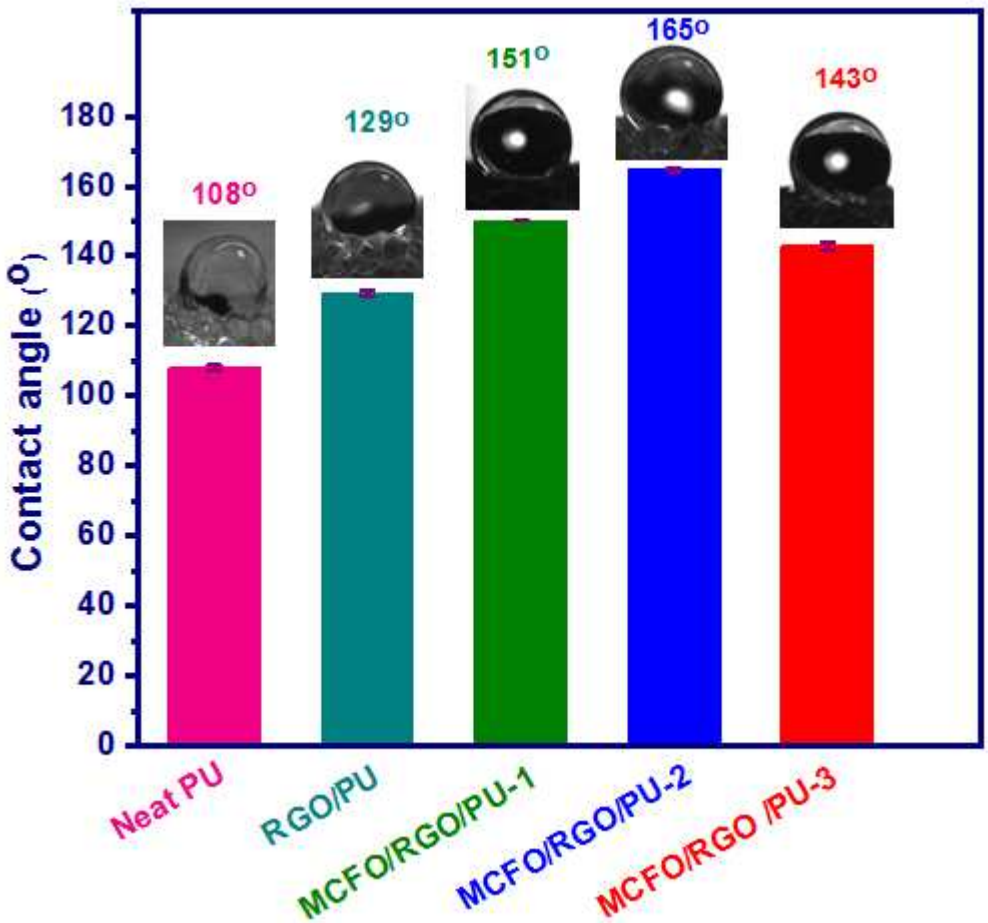

Figure 1. WCA values of neat PU and different MCFO/RGO/PU sponges.

To investigate the oleophilicity of MCFO/RGO/PU sponge, cooked oil was used. When cooked oil was dropped on the surface of the sponge, the oil droplet immediately spread out and meanwhile permeated into the porous structure of the sponge. Therefore, no contact angle could be measured, demonstrating the superoleophilicity of the MCFO/RGO/PU sponge (**Movie S1**). Owing to the superhydrophobicity and superoleophilicity of MCFO/RGO/PU sponge, it has a great potential for practical application in oil/water separation processes.

3.2.2. XRD, FTIR, Raman, XPS, and TEM analyses

The XRD patterns of GO and MCFO/RGO are depicted in **Figure S2**. The sharp peak at 2θ=10.85° in the XRD pattern of GO corresponds to the (002) crystalline plane with a large

interlayer distance of 8.2 Å due to the presence of oxygen containing functional groups. This peak disappears for MCFO/RGO nanocomposite, confirming the partial recovery of graphitic crystal structure. Indeed, two new peaks at 24.36° and 42.98° assigned respectively to the (002) and (102) crystalline planes of RGO appeared. The XRD pattern of MCFO/RGO comprises six characteristic diffraction peaks at 2θ=18.48°, 30.06°, 35.55°, 53.86°, 56.95°, and 62.67° attributed respectively to the (111), (220), (311), (422), (511), and (440) lattice planes. These peaks indicate magnetite Fe_3O_4 phase formation (JCPDS-96-900-9770) [27]. The two peaks at 2θ=44.50° and 47.65° correspond respectively to the (002) and (101) crystalline planes of hcp-Co (JCPDS-96-901-0968) [28]. In addition, the peak at about 2θ=42.98° (400) (JCPDS-96-153-9040) is ascribed to cubic-Mn [29]. The atomic ratio of Mn and Co was calculated by ICP analysis. The presence of magnetite Fe_3O_4 phase and the atomic ratio of Co and Mn elements (0.90:0.01), determined from ICP analysis, suggest the formation of $Mn_{0.01}Co_{0.90}Fe_3O_4$.

The FTIR spectra of GO, RGO, and magnetic MCFO/RGO are displayed in **Figure S3**. The FTIR spectrum of GO shows bands at 3381, 1726, 1620, 1383, 1228, and 1054 cm^{-1} ascribed respectively to O-H, C=O carboxyl, C=C in the aromatic ring, C-OH, epoxy C-O, and alkoxy C-O vibrations. The FTIR spectrum of RGO exhibits four weak bands at 3381, 1726, 1582, and 1052 cm^{-1} assigned respectively to O–H, C=O carboxyl, C=C, and alkoxy C-O vibration modes [15]. The C=C stretching mode of RGO was blue-shifted from 1620 to 1582 cm^{-1}, suggesting an increased structural ordering and restoration of sp^2 domains due to hydrothermal reduction of GO [30]. The FTIR spectrum of MCFO/RGO is composed of bands at 3381, 1620, 1390, and 680 cm^{-1} assigned to vibrations of O-H, C=C in the aromatic ring, Fe–O stretching mode of Fe_3O_4 [31], and Co(III)-O, respectively [32]. The bands at 1040, 1172, and 1230 cm^{-1} are related to the interactions among Mn, OH, and O groups atoms/groups [33, 34].

Figure S4 displays the Raman spectrum of MCFO/RGO with four obvious peaks of RGO, marked as D (1354 cm^{-1}), G (1586 cm^{-1}), 2D (2700 cm^{-1}), and D+G (2950 cm^{-1}) bands [35]. The G band is related to E_{2g} vibration mode of sp^2 carbon domains, whereas the D band arises from structural defects [36]. The 2D and D+G bands are due to the overtone of the D band and the combination mode induced by disorder, respectively [37]. Also, the peaks at around 663 and 672 cm^{-1} are characteristic of manganese oxide [38] and Fe_3O_4 NPs [39] , respectively. It is likely that both peaks are overlapped. The peak at 811 cm^{-1} is attributed to cobalt oxide [40]. There is an extra peak at 960 cm^{-1} due to silicon [41].

To assess the chemical composition, XPS analysis of MCFO/RGO nanocomposite was performed. **Figure S5a** depicts the XPS survey spectrum of MCFO/RGO, comprising peaks due to C 1s (285 eV), O 1s (532 eV), Mn 2p (642 eV), Fe 2p (710 eV), and Co 2p (781 eV), which is in a good agreement with the composition of the material. The atomic percentage of C 1s, O 1s, Co 2p, Fe 2p, and Mn 2p elements are 52.52, 32.75, 10.47, 3.77, and 0.49 at.%, respectively. The C 1s core level spectrum can be deconvoluted into four peaks at binding energies of 284.2, 285.1, 286.2, and 288.4 eV due to C=C, sp^3 C-C, epoxy and/or hydroxyl (C-O/C-OH), and carboxyl (O-C=O) functional groups, respectively (**Figure S5b**). The O 1s spectrum was curve-fitted with two peaks at binding energies of 531.5 and 532.8 eV assigned to epoxy (C-O) and hydroxyl (C–OH) groups, respectively (**Figure S5c**). As shown in **Figure S5d**, the high-resolution spectrum of the Mn 2p contains a pair of peaks located at about 642.2 and 653.6 eV attributed respectively to Mn $2p_{3/2}$ and Mn $2p_{1/2}$. The Mn $2p_{3/2}$ peak is deconvoluted into three peaks at 640.4, 642.1, and 643.5 eV related to Mn^{2+}, Mn^{3+}, and Mn^{4+} valence states, respectively [42]. The Mn $2p_{1/2}$ peak can be fitted with three peaks at binding energies of 651.1, 652.7, and 654.1 eV due to Mn^{2+}, Mn^{3+} and Mn^{4+} valence states, respectively [42-44]. Also, two satellites are observed at 646.1 and 659.3 eV [42, 45]. The Mn peak in the survey spectrum is weak, indicating that the content of Mn ions in

MCFO/RGO is low and Mn ions are doped into the interior of the nanocomposite. **Figure S5e** illustrates the Fe 2p XPS core level spectrum, which is deconvoluted in two main peaks including Fe $2p_{3/2}$ and Fe $2p_{1/2}$. Fe $2p_{3/2}$ can be fitted with three peaks at binding energies of 705.2, 709.9, and 712.1 eV which are the characteristic peaks of Fe^0, Fe^{2+}, and Fe^{3+}, respectively [46]. Fe $2p_{1/2}$ peak can be fitted with two peaks at 724.0 and 726.2 eV ascribed to Fe^{2+} and Fe^{3+}, respectively [47]. Moreover, two satellite peaks are observed at 719.1 and 733.1 eV which are due to Fe^{3+} and Fe^{2+} chemical states present in Fe_3O_4 phase [48]. The high-resolution spectrum of the Co 2p in **Figure S5f** shows characteristic peaks of Co at about 781.3 eV (Co $2p_{3/2}$) and 796.1 eV (Co $2p_{1/2}$). The Co $2p_{3/2}$ spectrum can be deconvoluted into two peaks at 781.0 and 783.6 eV that are the characteristic peaks for Co^{3+} $2p_{3/2}$ and Co^{2+} $2p_{3/2}$, respectively. In addition, the deconvolution of Co $2p_{1/2}$ shows two peaks at 796.2 and 798.4 eV which correspond to Co^{3+} $2p_{1/2}$ and Co^{3+} $2p_{1/2}$, respectively. Also, two satellites are observed at 787.0 and 803.2 eV [49].

The TEM images of GO and MCFO/RGO nanocomposite are exhibited in **Figure S6**. The TEM of GO displays a characteristic crumpled surface. The TEM of MCFO/RGO shows the presence of MCFO nanospheres with a size of 3-6 nm attached onto RGO sheets.

3.2.3. XRD and FTIR of MCFO/RGO/PU sponge

The XRD patterns of neat PU and MCFO/RGO/PU sponges are depicted in **Figure S7**. The peak at 2θ=20.7° in the XRD pattern of neat PU corresponds to the (110) crystalline plane [50]. In addition, the characteristic peaks of MCFO/RGO nanocomposite and PU sponges are clearly observed in MCFO/RGO/PU sponge XRD pattern. A very strong broad amorphous peak at about 2θ=20.7° is ascribed to the (110) plane and related to the disordered structure of the PU matrix amorphous phase [51]. Besides, the observed diffraction peaks at 2θ values of 18.48°, 24.36°, 30.06°, 35.55°, 42.98°, 44.50°, 47.65°, 53.6°, 56.95°, and 62.67° corresponding respectively to the lattice planes of (111), (002), (220), (311), (400), (002),

(101), (422), (511), and (440) indicate that the MCFO/RGO nanocomposite was successfully loaded onto the PU sponge surface.

The FTIR spectra of neat PU and MCFO/RGO/PU sponges are displayed in **Figure S8**. The neat PU sponge shows some distinguished bands at 3270 cm^{-1} ($\nu_{N-H,}$ ν_{O-H}), 2850–2970 (νs $_{C-H}$, $-CH_3$ and $-CH_2$), 2271 cm^{-1} (ν_{as} -NCO-), 1722 cm^{-1} (ν_{C-O} in the amide), 1637 cm^{-1} ($\nu_{C=O}$ in the urea), 1529 cm^{-1} ($\nu_{C=C}$), 1445 cm^{-1} (C–H deformation), 1072 cm^{-1} (ν_{C-O-C}), and 671 cm^{-1} (bending vibration of C–H) [52]. The FTIR spectrum of MCFO/RGO/PU sponge displays the same characteristic bands and positions like neat PU except for -NCO group. PU could form chemical bonds with materials through the NCO group of isocyanates. The absence of -NCO group in the FTIR spectrum of the modified PU sponge obviously demonstrates that the MCFO/RGO nanocomposite could be anchored on the PU surface effectively.

3.2.4. SEM images of neat PU, RGO/PU, MCFO/RGO/PU sponges

The SEM images of neat PU, RGO/PU, and magnetic MCFO/RGO/PU sponges are displayed in **Figure 2**. As shown in **Figure 2a**, the interconnected 3D porous structure of neat PU with a pore size ranging 100-500 μm makes it appropriate for sorption and storage of oil pollutants. Also, the smooth (absence of wrinkles) surface of the neat PU is obvious in its high magnification image (**Figure 2b**). As displayed in **Figure 2c** and **2d**, the surface of RGO/PU sponge exhibits higher roughness with respect to that of neat PU. From the SEM images in **Figure 2e** and **2f**, it is obvious that the MCFO/RGO/PU sponge maintains its porous structure with numerous tiny pores with respect to neat PU. It makes it appropriate for emulsion breakage. From the enlarged image of modified PU (**Figure 2g**), numerous irregular particles can be observed on the surface compared with the neat PU. This results in an enhancement of surface roughness and increase of superhydrophobic/superoleophilic property. In addition, compared with neat PU and RGO/PU sponges, such hierarchical

roughness could effectively reduce the diameter of sponge pores to the diameter of toluene/water emulsion droplets' size.

The EDS spectrum of MCFO/RGO/PU sponge in **Figure S9** demonstrates the presence of Co, Fe, Mn, O, and C elements in the modified sponge in good agreement with the XPS analysis.

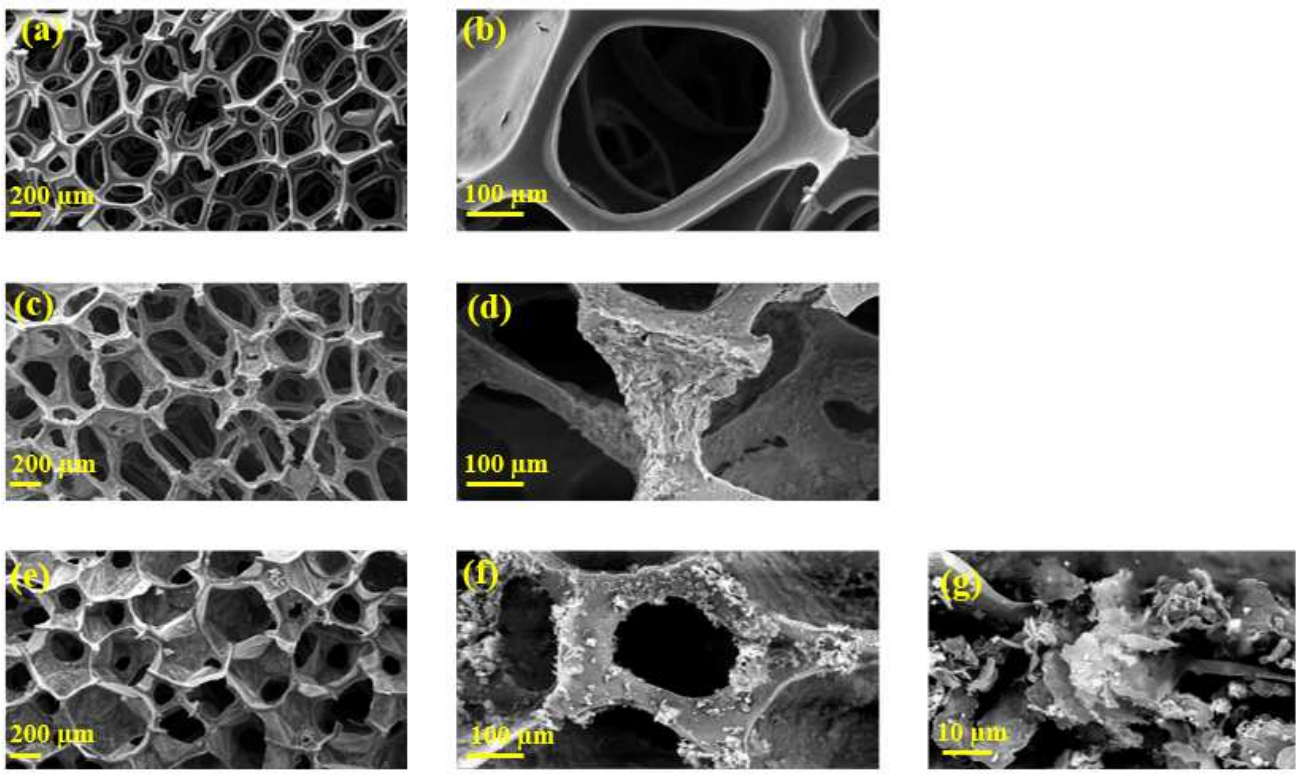

Figure 2. SEM images of (**a-b**) neat PU, (**c-d**) RGO/PU, and (**e-g**) MCFO/RGO/PU sponges.

Magnetic properties

The magnetic curves of the MCFO/RGO nanocomposite and MCFO/RGO/PU sponge are depicted in **Figure 3a**. The MCFO/RGO nanocomposite is ferromagnetic with remnant magnetization, M_r, coercivity, H_c, and specific saturation magnetization, M_s, of 0.63 emu g^{-1}, 20.0 Oe, and 22.05 emu g^{-1}, respectively. Also, the MCFO/RGO/PU sponge exhibited ferromagnetic property with M_r, H_c, and M_s of 0.14 emu g^{-1}, 30.0 Oe, and 2.72 emu g^{-1}, respectively. It is obvious that the magnetic property of MCFO/RGO/PU sponge is decreased

compared to that of MCFO/RGO nanocomposite due to the presence of relatively lower magnetic content. Nevertheless, the magnetic properties of MCFO/RGO/PU sponge are sufficient to manipulate the sponge using a magnet, as illustrated in **Figure 3b** and **movie S2**. **Figure 3c** and **movie S3** show the magnetic response of MCFO/RGO/PU sponge. The modified sponge can be easily driven to adsorb droplet of contaminant by using a magnet.

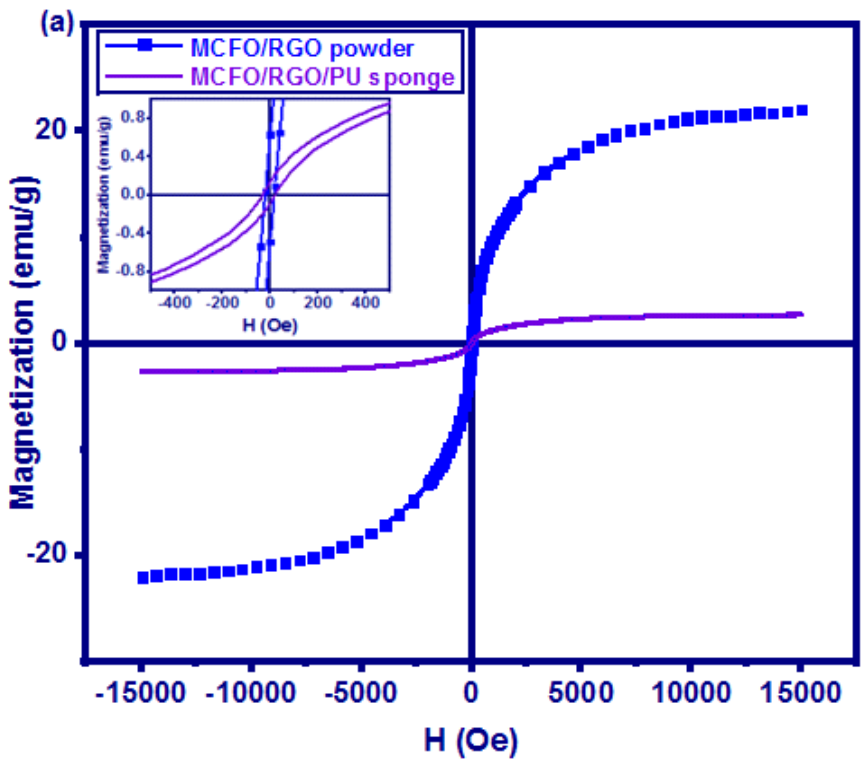

(b)

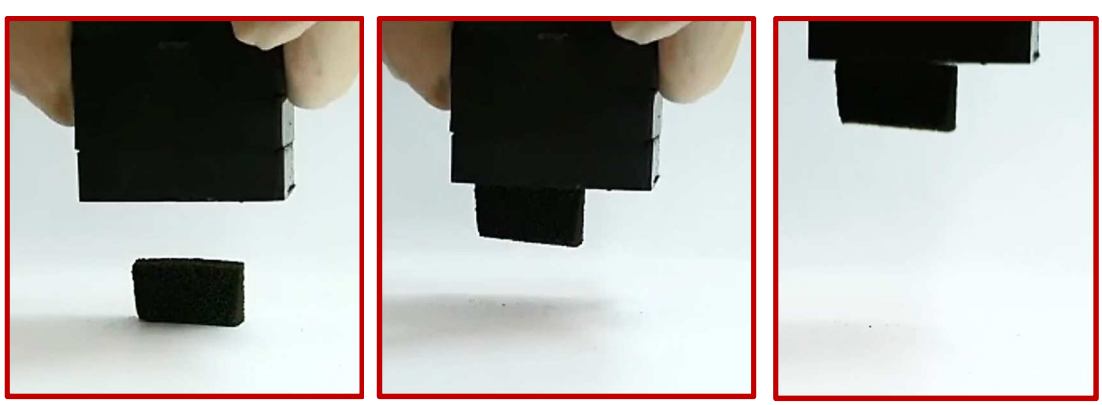

(c)

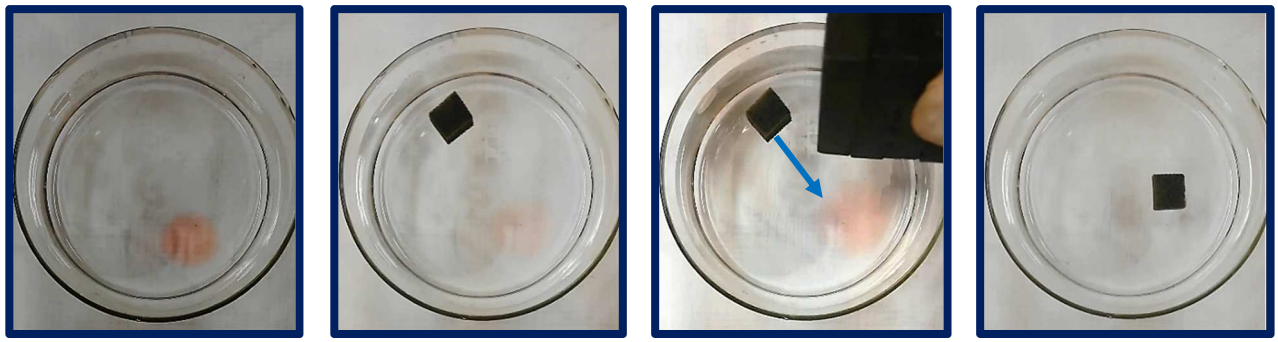

Figure 3. (**a**) Magnetization curves of MCFO/RGO nanocomposite and MCFO/RGO/PU sponge, (**b**) lifting the modified sponge *via* a magnet bar, and (**c**) the removal process of hydraulic oil by a piece of prepared sponge under a magnetic field.

3.4. MCFO/RGO/PU sponge stability in harsh conditions

Sorbent stability is an important factor in practical applications. **Figure S10a** confirms the excellent stability of the magnetic MCFO/RGO/PU sponge in harsh conditions including acidic, basic, and saline solutions upon immersion for 6 h at room temperature. In addition, the excellent stability property of the modified sponge was examined in a wide range of temperature from -4 to +140 ^{o}C. As shown in **Figure S10b**, the WCA is not significantly impacted by increasing the temperature except at 140 ^{o}C where a slight decrease in the WCA was observed (WCA=159±1^{o}). Therefore, the results prove the chemical and thermal stabilities of the modified MCFO/RGO/PU sponge, which guarantee its great potential for practical applications.

3.5. *Separation of oil/water mixtures using the MCFO/RGO/PU sponge*

In order to demonstrate the oil/water separation performance of the magnetic MCFO/RGO/PU sponge, a simple separation experiment was designed. The modified sponge was embedded in a funnel and a mixture of methylene blue-dyed water and dichloromethane was prepared and poured into the funnel (**Figure 4**). Although CH_2Cl_2 was successfully

separated from water by the sponge, organic solvents with lower density than water could not be easily separated.

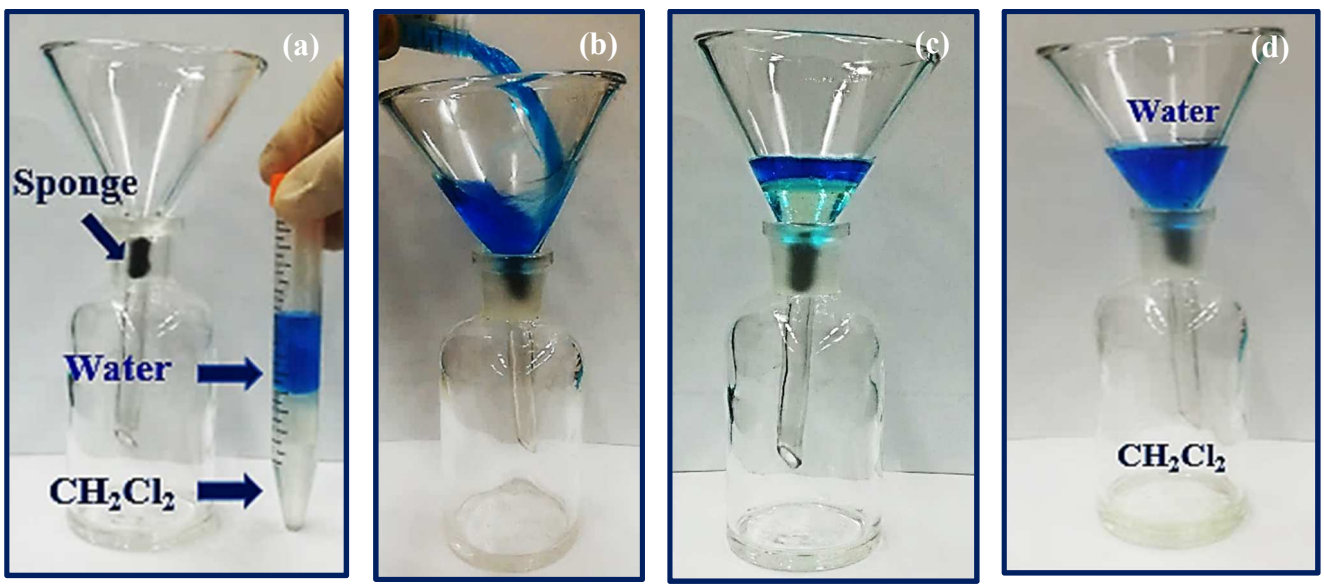

Figure 4. Snapshots of dichloromethane and colored water with methylene blue separation by MCFO/RGO/PU sponge.

The **movie S4** shows that the dichloromethane permeates through the MCFO/RGO/PU sponge rapidly, whereas the dyed water is maintained on top of the sponge, suggesting that the modified sponge has an excellent oil/water separation performance.

3.6. Magnetic property maintenance of MCFO/RGO/PU sponge underwater

To reveal the capability of magnetic response and oil/water separation of the MCFO/RGO/PU sponge, a methylene blue-dyed dichloromethane droplet is used as an oil spill underwater. As illustrated in **Figure 5**, the dichloromethane spill underwater could be rapidly adsorbed through an efficient magnetic drive by MCFO/RGO/PU sponge. Besides, the **movie S5** highlights that the functionalized sponge could effectively separate the oil droplet underwater and be handled by the magnet after oil sorption.

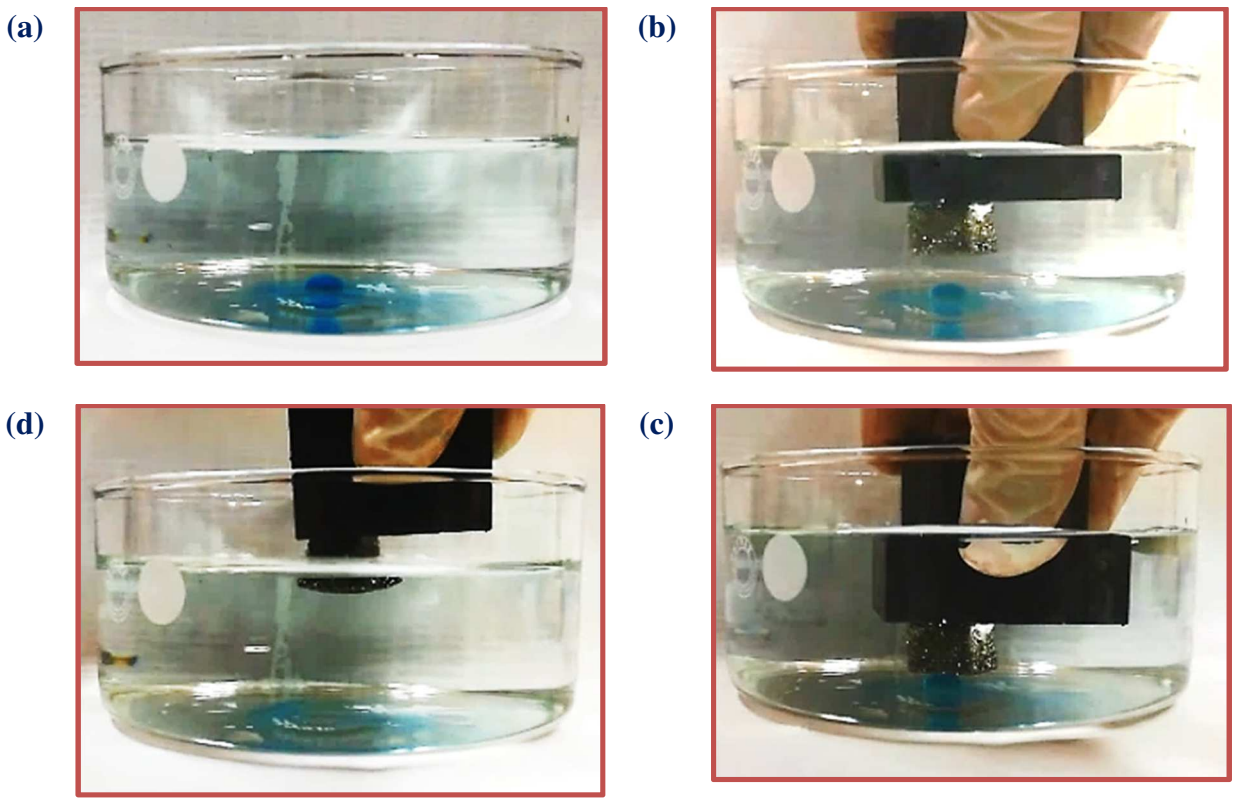

Figure 5. Snapshots of removal of methylene blue dyed underwater dichloromethane droplet by the MCFO/RGO/PU sponge using a magnet.

3.7. Sorption capacity and recyclability

The sorption capacity of neat PU, RGO/PU, and magnetic MCFO/RGO/PU sponges for oil and organic solvents including cooked oil, chloroform, ethyl acetate, toluene, and dichloromethane was determined to be in the range of 4.4-88.5, 33.5-98.0, and 39.8-131.4 g/g, respectively (**Figure 6a**). Hence, MCFO/RGO/PU sponge exhibits the best performance for sorption of oil and organic solvents due to the presence of several active sites on its surface. The variation of the sorption capacity of the MCFO/RGO/PU sponge for organic solvents and oils depends on their viscosity and density. The sorption capacity of RGO/PU for oils and organic solvents is greater than that of neat PU, whereas it is lower than that of MCFO/RGO/PU. Although RGO sheets enhance the hydrophobicity and oleophilicity of neat PU, at the same time, they fill some pores of PU. The performance of M□FO/RGO/PU sponge in comparison with other magnetic PU sponges is provided in **Table S1**. The

MCFO/RGO/PU prepared in this work has the greatest sorption capacity, which makes it as a promising sorbent for practical oil separation.

The recyclability of MCFO/RGO/PU sponge for five oil/organic solvents is investigated in **Figure 6b**. A simple mechanical squeezing method was used to desorb oils/organic solvents. The results showed that the MCFO/RGO/PU sponge could be recovered effectively, owing to its excellent mechanical property. The sorption capacity of MCFO/RGO/PU sponge did not change noticeably even after 10 sorption/desorption cycles (**Figure 6b**), which indicates its good structural stability.

XRD and SEM analysis of the MCFO/RGO/PU sponge after ten cycles of toluene sorption were performed. The XRD patterns of MCFO/RGO/PU sponge before and after ten sorption cycles of toluene are depicted in **Figure 6c**. The characteristic peaks of MCFO/RGO/PU sponge are clearly observed after ten sorption cycles, confirming the high stability of the sorbent. Besides, From the SEM images in **Figure 6d**, it is obvious that the MCFO/RGO/PU sponge maintained its porous structure after ten sorption cycles of toluene. In addition, from the enlarged images of the modified PU (**Figure 6e-g**), numerous irregular particles can be observed on the surface, indicating that the MCFO/RGO coating was not released from the PU surface after ten sorption cycles.

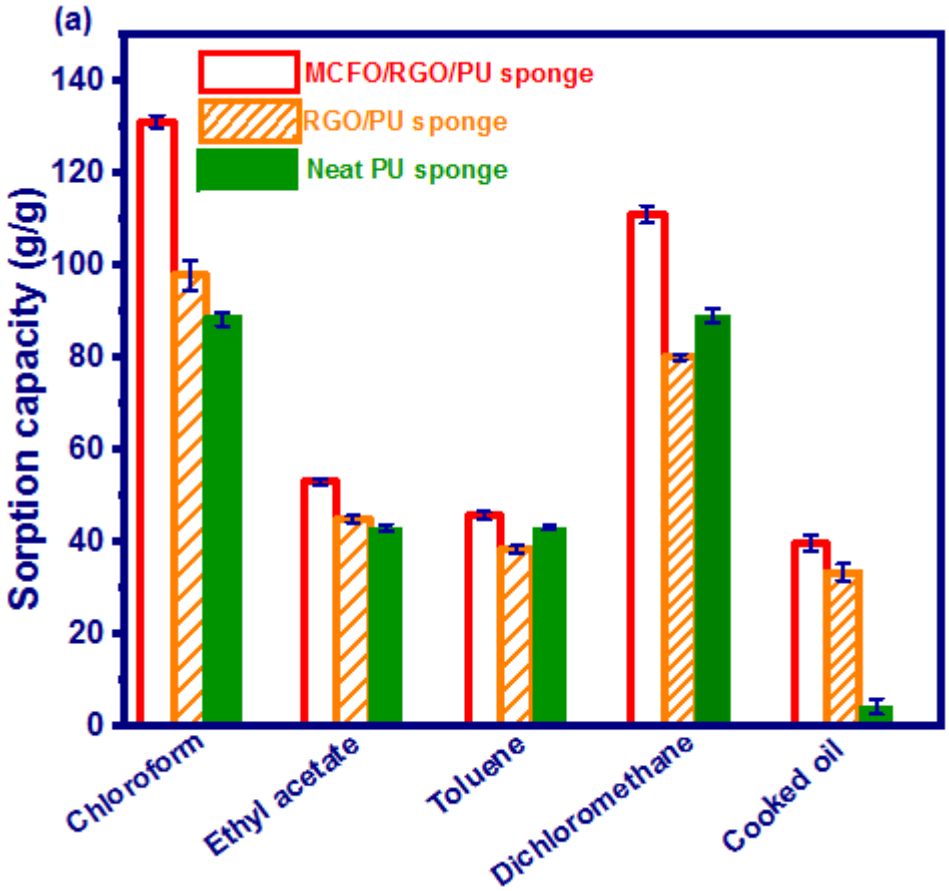
(a)
MCFO/RGO/PU sponge
RGO/PU sponge
Neat PU sponge
Sorption capacity (g/g)
0
20
40
60
80
100
120
140
Chloroform
Ethyl acetate
Toluene
Dichloromethane
Cooked oil

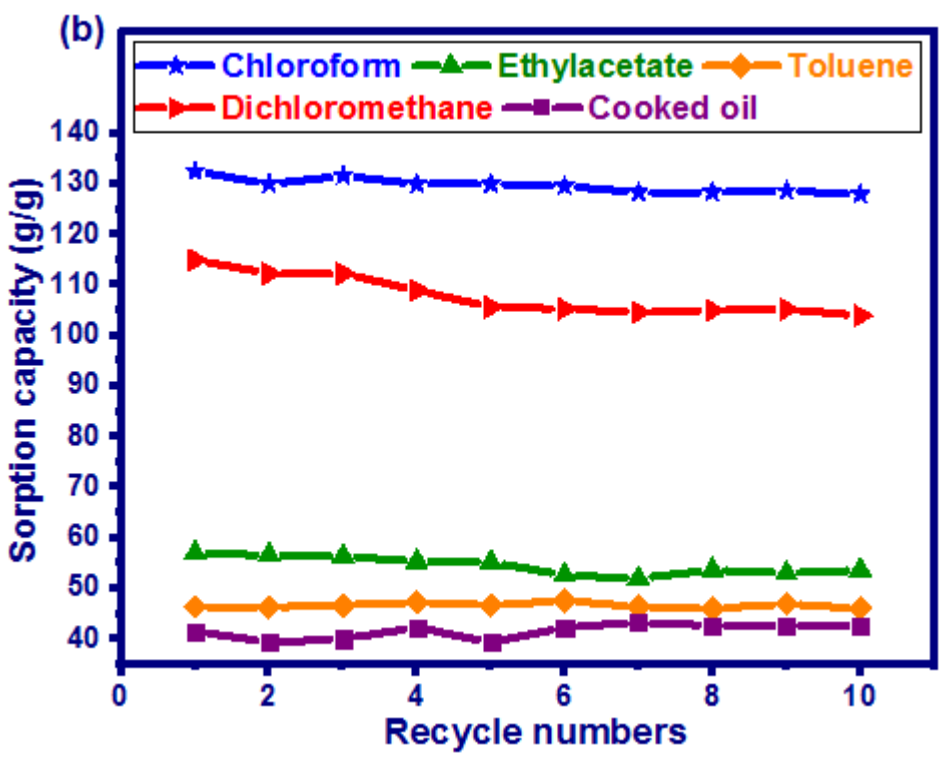
(b)
Chloroform
Ethylacetate
Toluene
Dichloromethane
Cooked oil
Sorption capacity (g/g)
40
50
60
70
80
90
100
110
120
130
140
0
2
4
6
8
10
Recycle numbers

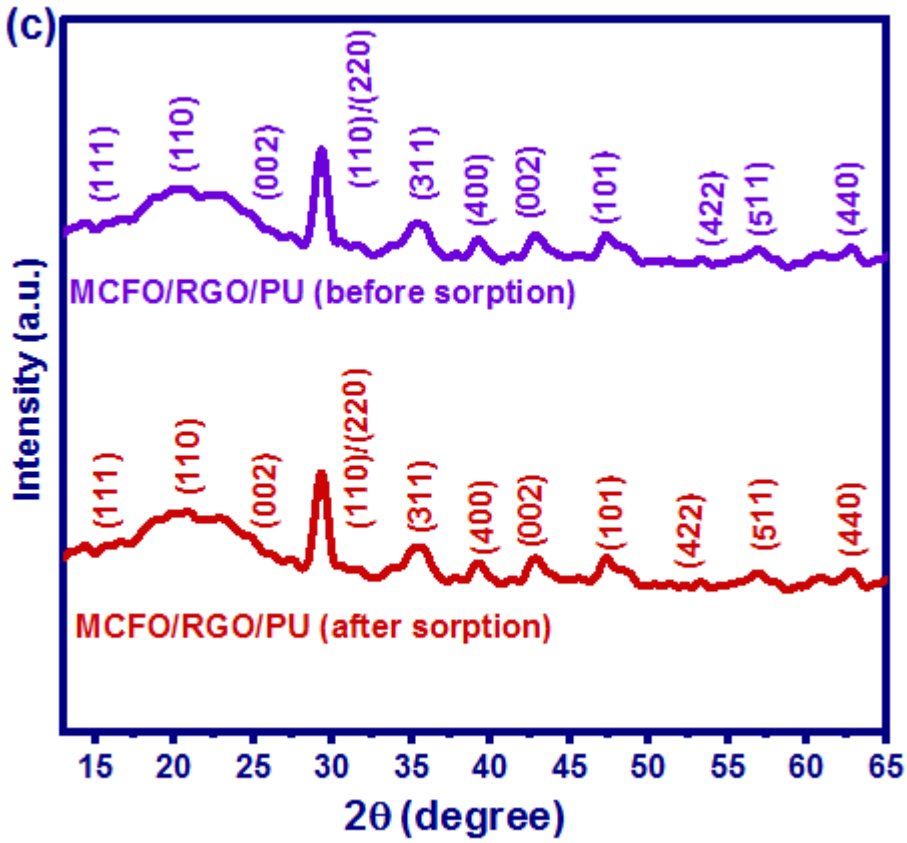

415

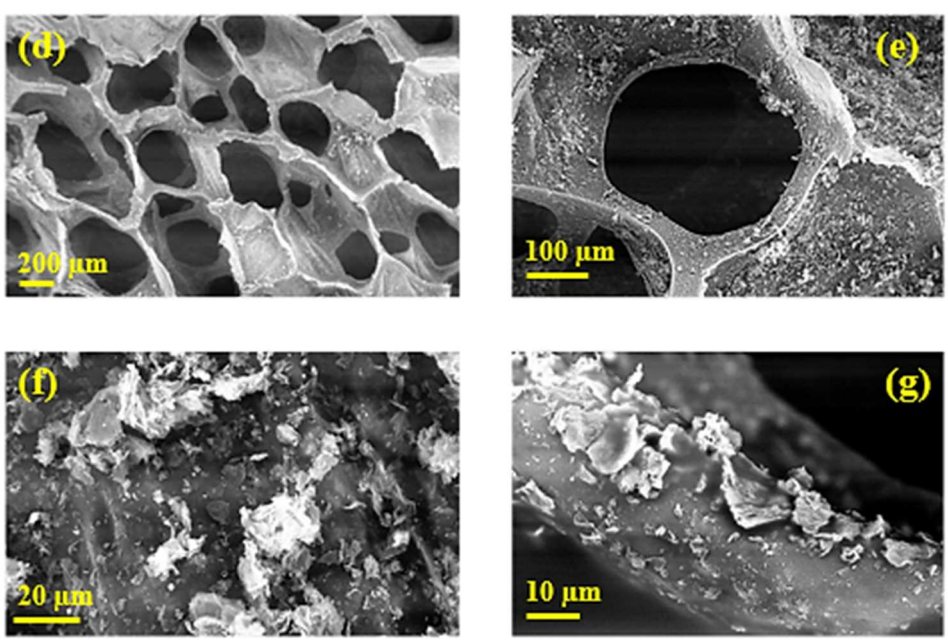

416

Figure 6. (**a**) The adsorption capacity of PU, RGO/PU, and MCFO/RGO/PU sponges for organic solvents and oils, (**b**) Recyclability of MCFO/RGO/PU for 10 adsorption cycles, (**c**) XRD patterns of MCFO/RGO/PU sponge before and after ten sorption cycles of toluene, and (**d-g**) SEM images of MCFO/RGO/PU sponge after ten sorption cycles of toluene.

417 418 419 420

421

3.8. Demulsification capacity of MCFO/RGO/PU sponge

The oil sewages, according to their diameter, *d*, can be classified into immiscible mixtures, unstable dispersions, and stable emulsions with $d < 20$ μm. The size mismatch between porous sponge (100-500 μm) and emulsified droplets limits the separation efficiency of sponges [1]. It is important to address this challenge while maintaining the high porosity of the sponges [19]. Herein, our strategy is to construct MCFO/RGO decorated PU surface, while preserving its intrinsic porous structure. As shown in SEM images (**Figure 2**), the MCFO/RGO nanocomposite could effectively reduce and match the diameter of sponge pores with that of toluene droplets in toluene/water emulsion. The MCFO/RGO/PU sponge could fully contact with emulsified water droplets, adsorb the toluene, and speed up the water coalescence. To investigate the demulsification ability of the MCFO/RGO/PU sponge, a W/O mixture was prepared by mixing 9 mL of toluene and 1 mL of water and sonicated for 1 h to produce a milky white colloid. In addition, O/W emulsion was prepared by addition of Pluronic F-127 (0.1 mg/mL in water) to toluene/water (1:9, v/v) and subsequently the mixture was emulsified under an ultrasonic bath for 1 h to prepare a milky white colloid. The MCFO/RGO/PU sponge was immersed in 4 mL emulsion until the emulsion became colorless. Before separation, the feeds of W/O and O/W mixtures were like a milky white liquid, as shown in **Figure 7a, b** left. After separation, the collected solutions were transparent compared to the feeds. The toluene content in the water phase was determined by UV-vis spectrophotometry (calibration curve in **Figure S11**). By immersion of the MCFO/RGO/PU sponge, a reduction in the toluene content (W/O) from 90% to 0.1% as well as (O/W) from 10% to 0.01% corresponding to toluene removal of 99.8% and 99.9%, respectively was achieved. It is worth to state that MCFO/RGO/PU sponge not only can separate the immiscible oil/water mixtures effectively, but it is also useful for emulsified oil/water mixtures especially in surfactant-stabilized emulsions.

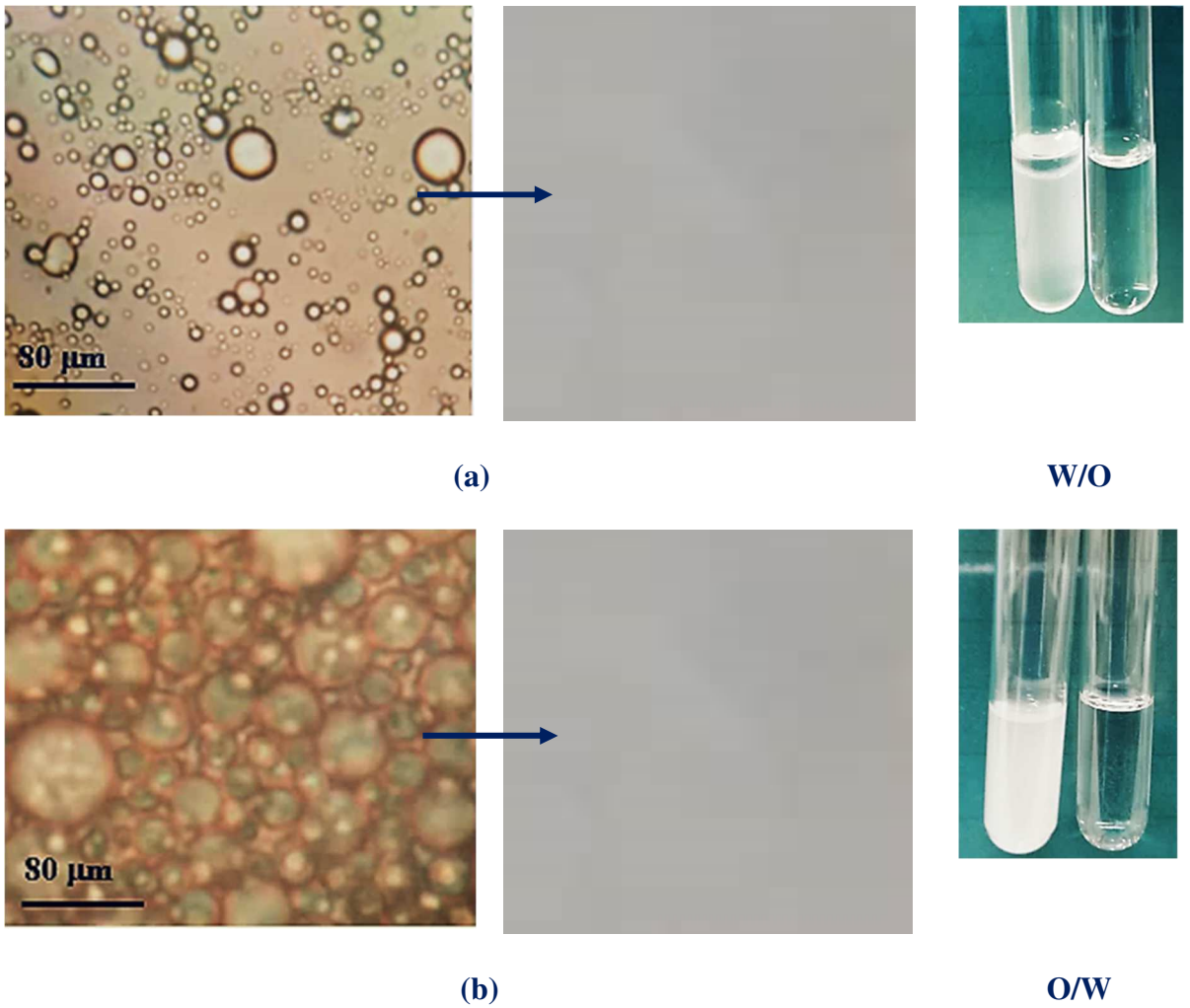

Figure 7. Optical photographs of surfactant-free water/toluene emulsion (W/O) and Pluronic F-127 emulsified toluene/water emulsion (O/W) (**a**) before and (**b**) after separation.

3.9. Surface energy estimate of MCFO/RGO/PU sponge

Determining the free-energy of solid surfaces has been an elusive attempt for surface scientists. The surface energy can be measured by Fowkes, Owens–Wendt, Zisman, and Girifalco–Good–Fowkes (GGF) approaches [53].

I. Fowkes theory

The Fowkes equation is expressed as follows:

$$\gamma_L(1+\cos\theta) = 2(\gamma_S^d \cdot \gamma_L^d)^{\frac{1}{2}} + 2(\gamma_S^p \cdot \gamma_L^p)^{\frac{1}{2}} \quad (2)$$

where θ is the contact angle of a liquid droplet on the solid surface, γ_L and γ_S refer respectively to surface energies of the liquid and solid calculated using Eq.3, d and h superscripts correspond to the dispersive and polar forces, respectively.

$$\gamma_{L(S)} = \gamma_{L(S)}^{d} + \gamma_{L(S)}^{P} \quad (3)$$

In order to calculate the surface energy, polar and nonpolar liquids should be considered. The values of γ_L^d and γ_L^P can be obtained from the literature [54]. The surface energy of the magnetic MCFO/RGO/PU sponge was determined by testing different combinations including water/diiodomethane, water/hexadecane, glycerol/diiodomethane, and glycerol/hexadecane. The average contact angle values of 4 μL liquid droplets are reported in **Table 1**. Upon substitution of these values into Eq. 2, two equations with two unknowns of γ_S^p and γ_S^d were solved. The surface energy, γ_S, of the magnetic MCFO/RGO/PU sponge was calculated as 48.36 mN·m^{-1} (γ_S^p = 9.16 mN·m^{-1} and γ_S^d= 39.2 mN·m^{-1}). The surface tension values of the polar and nonpolar liquids are exhibited in **Table 1**.

Table 1. Surface tension of various liquids and their corresponding contact angles (CAs) on the magnetic MCFO/RGO/PU sponge surface.

Liquid	γ_L^P/m N·m^{-1}	γ_L^d/mN·m^{-1}	γ_L/mN·m^{-1}	*CA* ($\pm I^o$)
Water	51.0	21.8	72.8	165
Glycerol	26.4	37.0	63.4	92
DI Water +Ethanol (95/05%)	-	-	59.0	85
Formamide	18.7	39.5	58.2	84
DI Water +Ethanol (90/10%)	-	-	52.0	75
Ethylene-glycol	19.0	29.0	48.0	70
DI Water +Ethanol (85/15%)	-	-	46.0	66
DI Water +Ethanol (80/20%)	-	-	43.0	60
Ethanol	2.6	18.8	22.4	0
Diiodomethane	0.0	50.8	50.8	0
Hexadecane	0.0	27.6	27.6	0

Dodecane	0.0	25.4	25.4	0
Decan	0.0	23.8	23.8	0

II. Owens–Wendt theory

The Owens–Wendt theory or extended Fowkes equation:

$$\frac{\gamma_l(1+\cos\theta)}{2\,(\gamma_L^d)^{\frac{1}{2}}} = (\gamma_S^p)^{\frac{1}{2}}\frac{(\gamma_L^p)^{\frac{1}{2}}}{(\gamma_L^d)^{\frac{1}{2}}} + (\gamma_S^d)^{\frac{1}{2}} \quad (4)$$

The surface energy of the magnetic MCFO/RGO/PU sponge was determined by testing different combinations including water/diiodomethane, water/hexadecane, glycerol/diiodomethane, and glycerol/hexadecane. The surface energy, γ_S, of the magnetic MCFO/RGO/PU sponge was calculated as 49.4 mN·m^{-1} (γ_S^p = 9.7 mN·m^{-1} and γ_S^d = 39.7 mN·m^{-1}).

III. Zisman model

The Zismen equation is expressed as follows:

$$\gamma_s = \frac{(b\gamma_c + 1)^2}{4b} \quad (5)$$

where, b is the slope of the fitted line.

Figure S12 displays the linear fitting of data by the Zisman equation of $cos\,\theta$ versus γ_L for liquids including glycerol, DI water + ethanol (95/05%), ethylene-glycol, DI water + ethanol (90/10%), DI water + ethanol (85/15%), DI water + ethanol (80/20%), and ethanol. The values of critical surface tension of wetting, γ_c, was obtained by extrapolating the linear curve to $cos\,\theta = 1$. Finally, the surface energy, γ_S, of the magnetic MCFO/RGO/PU sponge was calculated using the Zisman equation (23.5 mN·m^{-1}).

IV. GGF theory

The GGF equation is expressed as follows:

$$\cos\theta = -1 + 2\left(\frac{\gamma_S^d}{\gamma_L}\right)^{\frac{1}{2}} \quad (6)$$

The γ_S^d of the magnetic MCFO/RGO/PU sponge was determined by testing alkane liquids including decane, dodecane, and hexadecane. The γ_S^d of the magnetic MCFO/RGO/PU sponge was calculated as 23. 2 $mN \cdot m^{-1}$.

These results clearly revealed that the Fowkes, Owens–Wendt, Zisman, and GGF methods are significantly dependent upon the choice of liquids for calculating the surface energy of a solid surface. In addition, Zisman method works well for nonpolar surfaces. Therefore, since the PU surface has some polar components, the surface energy calculated using the Zisman method is not accurate. Besides, the GGF and Zisman methods underestimate the dispersive component of the magnetic sponge.

The results indicate that the surface energy values, obtained from the Owens–Wendt and the Fowkes methods, are more accurate. In addition, it is obvious that the degree of wettability was mainly dependent on the surface tension of the liquids. Indeed, the contact angle of liquids increases and follows a linear relation with increasing the surface tension. As a result, the magnetic MCFO/RGO/PU sponge could extensively adsorb liquids with low surface tension and repel liquids especially water with high surface tension. On the other hand, although the degree of wettability was mainly dependent on the surface tension of the liquids, there are other factors that affect the WCA such as the liquid density. There is an obvious difference in density of ethylene glycol (1.11 g/cm^3) and diiodomethane (3.32 g/cm^3). Therefore, WCA does not follow a linear relationship with surface tension for these two liquids. The contact angle of ethylene glycol is 70° while that of diiodomethane is about 0°.

3.10. Flame retardancy

PU sponges generate a large extent of toxic gases like carbon monoxide and hydrogen cyanide. Their open-cell structure makes oxygen diffusing through the pores and provides

more combustion sites. Hence, it is challenging to produce a highly efficient flame retardant (FR) barrier with sufficient thickness to strengthen PU sponges against flame [55]. Generally, during the combustion of FRs, a charred layer is produced which can serve as a physical barrier to hinder heat from underlayer substrates. Recently, graphene and its derivatives like RGO have attracted much attention as FR to hinder the transfer of combustion gases into the inflammable polymer skeleton [15]. Indeed, because of the large surface area and lamellar structure of RGO, it is favorable to form a physical protective layer on the PU surface. However, its low decomposition temperature (less than 600 °C) greatly restricts RGO application as a fire retardant [56]. To address this issue, metal ions and metal oxides known as non-intumescent flame-retardant materials are used to reinforce the fire retardancy property of RGO. In addition, they can increase the compatibility of RGO with the PU skeleton [57]. In this work, the neat PU and MCFO/RGO/PU sponges were cut into equal size, exposed to fire and the combustion process was recorded. As shown in **Figure 8a**, the neat PU was ignited immediately and burned completely within 13 s by leaving a small amount of residue at the end of the test. Compared with neat PU sponge, the modified MCFO/RGO/PU sponge exhibited self-extinguished and greater thermal stability properties brought by RGO and $Mn_{0.01}Co_{0.90}Fe_3O_4$ content (**Figure 8b** and **Movie S5**).

Figure S13 illustrates the FTIR spectra of MCFO/RGO/PU sponge before and after burning. It is obvious that there is no significant change in the FTIR spectrum of MCFO/RGO/PU sponge after burning test. Therefore, benefiting from the synergistic fire retardancy of MCFO/RGO nanocomposite and PU sponge, the modified sponge revealed remarkable adaptability in fire environments.

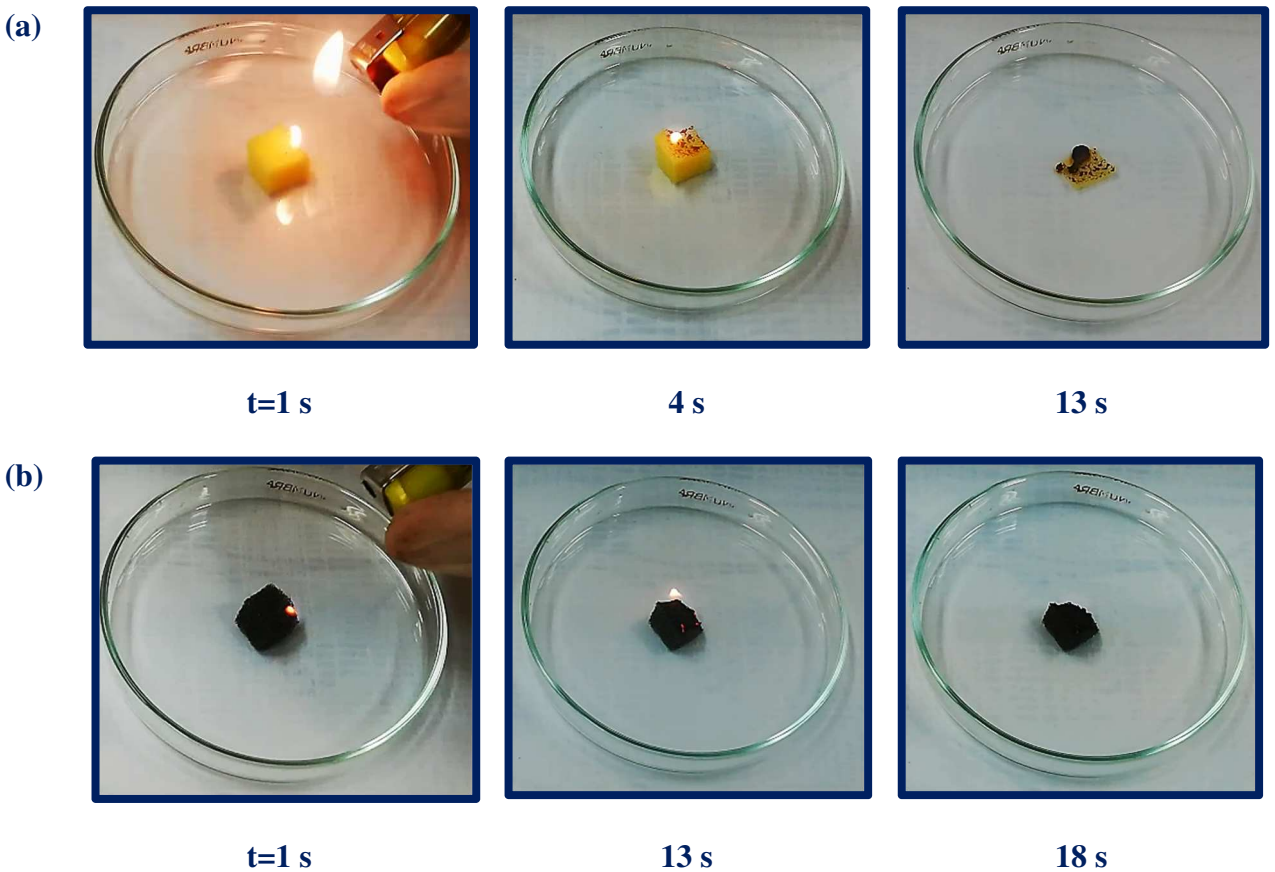

Figure 8. The snapshots of flammability test: (**a**) neat PU, (**b**) MCFO/RGO/PU sponges.

3.11. Mechanical stability of MCFO/RGO/PU sponge

The mechanical properties of MCFO/RGO/PU sponge are very important for practical applications in oil sorption. As shown in **Figure S14a-c**, water droplet still maintained a spherical shape under different mechanical deformation, including multiple times of substrate bending, compressing or twisting. The abrasion resistance of the MCFO/RGO/PU sponge (3×3×2 cm) was also examined. In this test, 200 g load was applied and the sponge was moved back/forth (an abrasion cycle) with abrasion length of about 5 cm. The WCA of the MCFO/RGO/PU sponge was recorded after various abrasion cycles. As shown in **Figure S15,** the WCA did not change obviously after every five abrasion cycles for a total of 20 cycles, indicating that the modified sponge possessed excellent superhydrophobicity and abrasion resistance. The insets in **Figure S15** show that the water droplets on MCFO/RGO/PU sponge still preserved a spherical shape with a WCA of 165°. This result confirmed that the

MCFO/RGO/PU sponge maintained its robust superhydrophobicity, because of the strong adhesion of the MCFO/RGO nanocomposite on the PU sponge surface.

4. Conclusion

A magnetic, superhydrophobic/superoleophilic, and flame-retardant $Mn_{0.01}Co_{0.90}Fe_3O_4$/reduced graphene oxide/polyurethane (MCFO/RGO/PU) sponge was fabricated through a simple dip-coating method. $Mn_{0.01}Co_{0.90}Fe_3O_4$/reduced graphene oxide (MCFO/RGO) nanocomposite was synthesized through *in situ* growth of magnetic MCFO nanoparticles on RGO *via* a solvothermal method. The nanocomposite decorated on PU skeleton could increase effectively the surface roughness and change the sponge wettability. The MCFO/RGO/PU sponge could be easily manipulated by a magnet and separate oil droplets from surfactant-free and stabilized toluene/water emulsions. Also, it could adsorb oils and organic solvents up to 131 times of its weight compared to neat PU sponge, while retaining its ability even after 10 sorption cycles. Additionally, the MCFO/RGO/PU sponge exhibited good mechanical and abrasion stability. Compared with neat PU, the robust magnetic MCFO/RGO/PU sponge exhibits self-extinguished property due to the presence of RGO in the nanocomposite anchored on PU matrix. The reported features make the modified PU as a promising candidate for remediation of oil spills.

Declaration of Competing Interest

The authors declare that they have no known competing financial interests or personal relationships that could have appeared to influence the work reported in this paper.

Acknowledgements

The authors would like to express their gratitude to Ferdowsi University of Mashhad for support of this project (Grant no. 3/48779). The authors gratefully acknowledge financial support from the Centre National de la Recherche Scientifique (CNRS), the University of Lille, and the Hauts-de-France region. ICP analyses were performed in the « Spectrométrie

579 par torche à plasma » platform of the Research Federation Michel-Eugène Chevreul hosted by
580 the LASIRE laboratory.

581 **References**

582 [1] W. Zhang, N. Liu, Y. Cao, X. Lin, Y. Liu, L. Feng, Superwetting porous materials for
583 wastewater treatment: from immiscible oil/water mixture to emulsion separation, Adv. Mater.
584 Interfaces 4 (2017) 1600029-1600047 .
585 [2] R.K. Gupta, G.J. Dunderdale, M.W .England, A. Hozumi, Oil/water separation
586 techniques: a review of recent progresses and future directions, J. Mater. Chem. A 5 (2017)
587 16025-16058. [3] Y. Hou, Z. Wang, J. Guo, H. Shen, H. Zhang, N. Zhao, Y. Zhao, L. Chen,
588 S. Liang, Y. Jin, Facile fabrication of robust superhydrophobic porous materials and their
589 application in oil/water separation, J. Mater. Chem. A 3 (2015) 23252-23260.
590 [4] A. Laborel-Préneron, C. Magniont, J.-E. Aubert, Characterization of barley straw, hemp
591 shiv and corn cob as resources for bioaggregate based building materials, Waste Biomass
592 Valorization 9 (2018) 1095-1112 .
593 [5] M. Vintu, G. Unnikrishnan, Indolocarbazole based polymer coated super adsorbent
594 polyurethane sponges for oil/organic solvent removal, J. Environ. Manage. 248 (2019)
595 109344-109355.
596 [6] M. Khosravi, S. Azizian, Synthesis of a novel highly oleophilic and highly hydrophobic
597 sponge for rapid oil spill cleanup, ACS Appl. Mater. Interfaces 7 (2015) 25326-25333.
598 [7] Q. Zhu, Y. Chu, Z. Wang, N. Chen, L. Lin, F. Liu, Q. Pan, Robust superhydrophobic
599 polyurethane sponge as a highly reusable oil-absorption material, J. Mater. Chem. A 1 (2013)
600 5386-5393.
601 [8] B. Ge, Z. Zhang, X. Zhu, X. Men, X. Zhou, A superhydrophobic/superoleophilic sponge
602 for the selective absorption oil pollutants from water, Colloids Surf., A 457 (2014) 397-401.

603 [9] N. Cao, B. Yang, A. Barras, S. Szunerits, R. Boukherroub, Polyurethane sponge
604 functionalized with superhydrophobic nanodiamond particles for efficient oil/water
605 separation, Chem. Eng. J. 307 (2017) 319-325.

606 [10] Y. Tang, H. Huang, X. Guo, C. Zhong, Superhydrophobic Ether-Based Porous Organic
607 Polymer-Coated Polyurethane Sponge for Highly Efficient Oil–Water Separation, Ind. Eng.
608 Chem. Res. 59 (2020) 13228-13238.

609 [11] A. Andersson, A. Magnusson, S. Troedsson, S. Lundmark, F.H. Maurer, Intumescent
610 foams - a novel flame retardant system for flexible polyurethane foams, J. Appl. Polym. Sci.
611 109 (2008) 2269-2274.

612 [12] F. Zhou, T. Zhang, B. Zou, W. Hu, B. Wang, J. Zhan, C. Ma, Y. Hu, Synthesis of a novel
613 liquid phosphorus-containing flame retardant for flexible polyurethane foam: Combustion
614 behaviors and thermal properties, Polym. Degrad. Stab. 171 (2020) 109029-109065.

615 [13] J. Wang, H. Wang, G. Geng, Flame-retardant superhydrophobic coating derived from fly
616 ash on polymeric foam for efficient oil/corrosive water and emulsion separation, J. Colloid
617 Interface Sci. 525 (2018) 11-20.

618 [14] N. Yousefi, X. Lu, M. Elimelech, N. Tufenkji, Environmental performance of graphene-
619 based 3D macrostructures, Nature Nanotechnol. 14 (2019) 107-119.

620 [15] A. Jamsaz, E.K. Goharshadi, Flame retardant, superhydrophobic, and superoleophilic
621 reduced graphene oxide/orthoaminophenol polyurethane sponge for efficient oil/water
622 separation, J. Mol. Liq. 307 (2020) 112979-112991.

623 [16] X. Lü, Z. Cui, W. Wei, J. Xie, L. Jiang, J. Huang, J. Liu, Constructing polyurethane
624 sponge modified with silica/graphene oxide nanohybrids as a ternary sorbent, Chem. Eng. J.
625 284 (2016) 478-486.

626 [17 N. Chen, Q. Pan, Versatile fabrication of ultralight magnetic foams and application for
627 oil–water separation, ACS nano 7 (2013) 6875-6883.

628 [18] T. Yu, F. Halouane, D. Mathias, A. Barras, Z. Wang, A. Lv, S. Lu, W. Xu, D. Meziane,
629 N. Tiercelin, Preparation of magnetic, superhydrophobic/superoleophilic polyurethane
630 sponge: Separation of oil/water mixture and demulsification, Chem. Eng. J. 384 (2020)
631 123339-123348.
632 [19] Y. Liu ,X. Wang, S. Feng, Nonflammable and magnetic sponge decorated with
633 polydimethylsiloxane brush for multitasking and highly efficient oil–water separation, Adv.
634 Funct. Mater. 29 (2019) 1902488-1902500.
635 [20] W. Kang, Y. Cui, L. Qin, Y. Yang, Z. Zhao, X. Wang, X. Liu, A novel robust adsorbent
636 for efficient oil/water separation: Magnetic carbon nanospheres/graphene composite aerogel,
637 J. Hazard. Mater. 392 (2020) 122499-122512.
638 [21] O. Guselnikova, A. Barras, A. Addad, E. Sviridova, S. Szunerits, P. Postnikov, R.
639 Boukherroub, Magnetic polyurethane sponge for efficient oil adsorption and separation of oil
640 from oil-in-water emulsions, Sep. Purif. Technol. 240 (2020) 116627-116625.
641 [22] Y. Liu, J.-C. Zhao, C.-J. Zhang, Y. Guo, P. Zhu, D.-Y. Wang, Effect of manganese and
642 cobalt ions on flame retardancy and thermal degradation of bio-based alginate films, J. Mater.
643 Sci. 51 (2016) 1052-1065.
644 [23] H. Wang, J.T. Robinson, G. Diankov, H. Dai ,Nanocrystal growth on graphene with
645 various degrees of oxidation, J. Am. Chem. Soc. 132 (2010) 3270-3271.
646 [24] C. Peng, B. Chen, Y. Qin, S. Yang, C. Li, Y. Zuo, S. Liu, J. Yang, Facile ultrasonic
647 synthesis of CoO quantum dot/graphene nanosheet composites with high lithium storage
648 capacity, ACS nano 6 (2012) 1074-1081
649 [25] R. Zan, U. Bangert, Q. Ramasse, K.S. Novoselov, Metal– graphene interaction studied
650 via atomic resolution scanning transmission electron microscopy, Nano Lett. 11 (2011) 1087-
651 1092.

652 [26] Z. Zhang, Y. Wang, D. Li, Q. Tan, Y. Chen, Z. Zhong, F. Su, Mesoporous $Mn_{0.5}Co_{0.5}Fe_2O_4$ nanospheres grown on graphene for enhanced lithium storage properties, Ind. Eng.
654 Chem. Res. 52 (2013) 14906-14912.
655 [27] H. El Ghandoor, H. Zidan, M.M. Khalil, M. Ismail, Synthesis and some physical
656 properties of magnetite (Fe_3O_4) nanoparticles, Int. J. Electrochem. Sci 7 (2012) 5734-5745.
657 [28] M.A. Kashi, M. Ghaffari, F. Torshizi, Structural and magnetic tunability of Co/Cu
658 multilayer nanowires induced by electrolyte acidity and spacer layer thickness, J. Alloys
659 Compd. 820 (2020) 153087-153099.
660 [29] X. Zhu, H. Zhao, X. Niu, T. Liu, L. Shi, M. Lan, A comparative study of carbon
661 nanotube supported MFe_2O_4 spinels (M= Fe, Co, Mn) for amperometric determination of
662 H_2O_2 at neutral pH values, Microchim. Acta 183 (2016) 2431-2439.
663 [30] P. Bansal, A. Panwar, D. Bahadur, Effect of reaction temperature on structural and
664 optical properties of reduced graphene oxide, Int. J. Mater., Mech. Manuf. 2 (2014) 18-20.
665 [31] D.V. Quy, N.M. Hieu, P.T. Tra, N.H. Nam, N.H. Hai, N. Thai Son, P.T. Nghia, N.T.V.
666 Anh, T.T. Hong, N.H. Luong, Synthesis of silica-coated magnetic nanoparticles and
667 application in the detection of pathogenic viruses, J. Nanomater. 2013 (2013) 603940-603946.
668 [32] E.A. Aboelazm, G.A. Ali, K.F. Chong, Cobalt oxide supercapacitor electrode recovered
669 from spent lithium-ion battery, Chem. Adv. Mater. 3 (2018) 67-74.
670 [33] M. Mylarappa, V.V. Lakshmi, K.V. Mahesh, H. Nagaswarupa, N. Raghavendra, A facile
671 hydrothermal recovery of nano sealed MnO_2 particle from waste batteries: An advanced
672 material for electrochemical and environmental applications, IOP Conf. Series: Materials
673 Science and Engineering, 149 (2016) 12178-12188.
674 [34] R. Ali, S. Adil, A. Al-warthan, M.R.H. Siddiqui, Identification of active phase for
675 selective oxidation of benzyl alcohol with molecular oxygen catalyzed by copper-manganese
676 oxide nanoparticles, J. Chem. 2013 (2013) 367261-367269.

[35] S. Gupta, J. Narayan, Non-equilibrium processing of ferromagnetic heavily reduced graphene oxide, Carbon 153 (2019) 663-673.

[36] M. B. Moghaddam, E.K. Goharshadi, M.H. Entezari, P. Nancarrow, Preparation, characterization, and rheological properties of graphene–glycerol nanofluids, Chem. Eng. J. 231 (2013) 365-372.

[37] M. Hadadian, E.K. Goharshadi, A. Youssefi, Electrical conductivity, thermal conductivity, and rheological properties of graphene oxide-based nanofluids, J. Nanopart. Res. 16 (2014) 2788-2805.

[38] A. Pramanik, S. Maiti, M. Sreemany, S. Mahanty, Rock-Salt-Templated Mn_3O_4 Nanoparticles Encapsulated in a Mesoporous 2D Carbon Matrix: A High Rate 2 V Anode for Lithium-Ion Batteries with Extraordinary Cycling Stability, ChemistrySelect 2 (2017) 7854-7864.

[39] Q. Zhang, B. Wu, R. Song, H. Song, J. Zhang, X. Hu, Preparation, characterization and tribological properties of polyalphaolefin with magnetic reduced graphene oxide/Fe_3O_4, Tribol. Int. 141 (2020) 105952-105962.

[40] C. W. Tang, C.-B. Wang, S.-H. Chien, Characterization of cobalt oxides studied by FT-IR, Raman, TPR and TG-MS, Thermochim. Acta 473 (2008) 68-73.

[41] A. Dhakal, P. Wuytens, A. Raza, N. Le Thomas, R. Baets, Silicon nitride background in nanophotonic waveguide enhanced Raman spectroscopy, Materials 10 (2017) 140-153.

[42] B. Sambandam, V. Soundharrajan, J. Song, S. Kim, J. Jo, P.T. Duong, S. Kim, V. Mathew, J. Kim, Investigation of Li-ion storage properties of earth abundant β-$Mn_2V_2O_7$ prepared using facile green strategy, J. Power Sources 350 (2017) 80-86.

[43] G. Zhao, X. Huang, X. Wang, P. Connor, J. Li, S. Zhang, J.T. Irvine, Synthesis and lithium-storage properties of MnO/reduced graphene oxide composites derived from graphene

oxide plus the transformation of Mn (VI) to Mn (II) by the reducing power of graphene oxide, J. Mater. Chem. A 3 (2015) 297-303.

[44] H. Chen, M.Q. Wang, Y. Yu, H. Liu, S.-Y. Lu, S.-J. Bao, M. Xu, Assembling hollow cobalt sulfide nanocages array on graphene-like manganese dioxide nanosheets for superior electrochemical capacitors, ACS Appl. Mater. Interfaces 9 (2017) 35040-35047.

[45] Y. Li, Z. Yang, H. Zhang, X. Tong, J. Feng, Fabrication of sewage sludge-derived magnetic nanocomposites as heterogeneous catalyst for persulfate activation of Orange G degradation, Colloids Surf. A 529 (2017) 856-863.

[46] Y. Dai, M. Chen, X. Yan, J. Wang, Q. Wang, C. Zhou, D. Wang, H. Zhang, Y. Wang, X. Cheng, Ultra-Small Fe_3O_4 Nanoparticles Decorated WS_2 Nanosheets with Superior Electrochemical Properties for Supercapacitors, J. Nanosci. Nanotechnol. 19 (2019) 897-904.

[47] Z. Na, R. Yao, Q. Yan, X. Wang, X. Sun, X. Wang, A general strategy for enabling Fe_3O_4 with enhanced lithium storage performance: Synergy between yolk-shell nanostructures and doping-free carbon, Electrochim. Acta (2020) 137464-137471.

[48] A. Gangwar, A. Sharma, S. Shaw, S.S. Meena, N. Prasad, Structural and electrochemical performance studies for nanocomposites of carbon with Fe_3C or Mn-Substituted (Fe_3C/Fe_3O_4) as anodes for Li-batteries, Appl. Surf. Sci. 533 (2020) 147474-147484.

[49] C. Zhang, X. Cai, Y. Qian, H. Jiang, L. Zhou, B. Li, L. Lai, Z. Shen, W. Huang, Electrochemically synthesis of nickel cobalt sulfide for high-performance flexible asymmetric supercapacitors, Adv. Sci. 5 (2018) 1700375-1700387..

[50] M. Maggira, E.A. Deliyanni, V.F. Samanidou, Synthesis of graphene oxide based sponges and their study as sorbents for sample preparation of cow milk prior to HPLC determination of sulfonamides, Molecules 24 (2019) 2086-2101.

[51] A.K. Barick, D.K. Tripathy, Preparation, characterization and properties of acid functionalized multi-walled carbon nanotube reinforced thermoplastic polyurethane nanocomposites, J. Mater. Sci. Eng. B 176 (2011) 1435-1447.

[52] A. Jamsaz, E.K. Goharshadi, An environmentally friendly superhydrophobic modified polyurethane sponge by seashell for the efficient oil/water separation, Process Saf. Environ. Prot. 139 (2020) 297-304.

[53] N. Selvakumar, H.C. Barshilia, K. Rajam, Effect of substrate roughness on the apparent surface free energy of sputter deposited superhydrophobic polytetrafluoroethylene coatings: A comparison of experimental data with different theoretical models, J. Appl. Phys. 108 (2010) 013505-013515.

[54] A. Zdziennicka, J. Krawczyk, K. Szymczyk, B. Jańczuk, Components and parameters of liquids and some polymers surface tension at different temperature, Colloids Surf. A 529 (2017) 864-875.

[55] E. Akdogan, M. Erdem, M.E. Ureyen, M. Kaya, Rigid polyurethane foams with halogen-free flame retardants: Thermal insulation, mechanical, and flame retardant properties, J. Appl. Polym. Sci. 137 (2020) 47611-47625.

[56] L. Dong, C. Hu, L. Song, X. Huang, N. Chen, L. Qu, A large-area, flexible, and flame-retardant graphene paper, Adv. Funct. Mater. 26 (2016) 1470-1476.

[57] S. Wang, R. Gao, K. Zhou, The influence of cerium dioxide functionalized reduced graphene oxide on reducing fire hazards of thermoplastic polyurethane nanocomposites, J. Colloid Interface Sci. 536 (2019) 127-134.